right ear. He was hospitalized twice for respiratory distress triggered by infections, which required placement of a tracheostomy tube at age 1 year. He had three surgical procedures for thoracolumbar kyphoscoliosis. Motor development was severely delayed: he sat at 9 months, pulled up to a stand at 2 6/12 years, crawled at 4 years, and walked with assistance from age 4 years. At age 10 years, he weighs 31.5 kg (50th percentile), has a height of 122 cm (3rd percentile), and an OFC of 52.5 cm (50th percentile). He speaks no words and is not toilet trained. He has hyperactivities.

ARID1B Mutations

ARID1B-1 (Subject 1 [Tsurusaki et al., 2012]; Fig. 6a–c): He was born at 39 weeks of gestation after an uncomplicated prenatal period. His birth weight was 2,760 g (−0.9 SD), length was 50 cm (+0.4 SD), and OFC was 34 cm (+0.3 SD). He had sucking/feeding difficulties and vomited frequently, resulting in failure to thrive. His feeding improved after 3 years of age. He suffered from atopic dermatitis and recurrent infections. He showed hypotonia and motor development was moderately delayed: he raised his head at age 6 months, sat alone at 1 year, and walked independently at 2 9/12 years. MRI of the brain at age 7 years showed hypoplasia of the corpus callosum. At age 13 years, he weighs 44 kg (−0.5 SD), has a height of 150 cm (−1.4 SD), and an OFC of 55 cm (+0.7 SD). Pes planus has become evident. He has difficulty in fine finger movement. He speaks no words but can write "kanji" (Chinese characters) and communicate in writing. He can also summate two-digit numbers. He has autism spectrum disorder with hyperactivity, impulsiveness, and an obsession with trains. He has normal secondary sexual characteristics and no susceptibility to infection.

ARID1B-2 (Subject 15 [Tsurusaki et al., 2012]; Fig. 6d–p): He was born at 40 weeks of gestation after an uncomplicated prenatal period. His birth weight was 2,620 g (−1.2 SD), length was 47.5 cm (−1.2 SD), and OFC was 32.0 cm (−1.1 SD). He had sucking/feeding difficulties. He showed hypotonia and motor development was delayed: he raised his head at 3–4 months, rolled over at 4–5 months, sat alone at 1 2/12 years, and walked independently at 2 10/12 years. MRI of the brain at age 2 years did not show abnormalities. He had three episodes of febrile seizures. He suffered from frequent upper respiratory infections with vomiting from age 5 years when his younger sister entered a nursery. He was suspected to have an autism spectrum disorder at age 3 years, and received risperidone for impulsiveness from age 6 years. At age 7 9/12 years, he weighs 20.4 kg (−1.1 SD), has a height of 118 cm (−1.1 SD), and an OFC of 50.3 cm (−1.4 SD). Though he speaks only "Ah, oh" in simple voices without meaningful words, he understands what he needs to do in his daily life and what his parents say, indicates what he wants, and answers yes–no questions by changing the tone of his voice. He is defiant, but seems to have become less autistic: he likes others, reads other people's faces, and settles quarrels. He becomes exhausted easily.

ARID1B-3 (Subject 23 [Tsurusaki et al., 2012]; Fig. 6q–s): Ventricular enlargement and a sacral cystic lesion were observed on fetal ultrasonography at 28 weeks of gestation. She was born at 38 weeks of gestation. Her birth weight was 2,966 g (+0.5 SD), length was 44.5 cm (−1.7 SD), and OFC was 33.8 cm (+0.4 SD). She had a deep sacral dimple without a neurological deficit. Oxygen was administered to treat transient tachypnea of the newborn, followed by inspiratory stridor caused by laryngomalacia. In infancy, she had sucking/feeding difficulties that resulted in failure to thrive. Obesity started at age 3 years. Obstructive apnea associated with hypertrophic tonsils and adenoids as well as allergic rhinitis developed, and was treated with medication. At age 4 years, intermittent exotropia and mild scoliosis with a Cobb angle of 2.5° at Th11–L3 were noted. MRI of the brain at age 5 years showed agenesis of the corpus callosum and colpocephaly. She showed hypotonia and motor development was delayed: she raised her head at age 7 months, sat alone at 1 year, walked independently at 2 8/12 years, and spoke one word after 2 years of age. The DQ at age 5 6/12 years was 36. She suffered from recurrent infections. At age 10 years, she weighs 40.9 kg (+1.5 SD), has a height of 128.3 cm (−1.3 SD), and an OFC of 56.2 cm (+1.8 SD). She practices reading, writing, and arithmetic, but is not good at speaking in public. She has difficulty in moving her left hand quickly compared with her right hand.

ARID1B-4 (Subject 10 [Tsurusaki et al., 2012]; Fig. 6t): He was born at 39 weeks of gestation. His birth weight was 2,730 g (−1.0 SD), length was 47 cm (−1.1 SD), and OFC was 34 cm (+0.3 SD). He had right cryptorchidism. He received thyroid hormone replacement for congenital hypothyroidism. He had sucking/feeding difficulties. He showed hypotonia and motor development was moderately delayed: he raised his head at age 7 months, sat alone at 1 6/12 years, and walked independently at 2 1/12 months. The DQ at age 6 years was 47. He suffered from occasional vomiting attacks. At age 11 years, he weighs 30 kg (−0.5 SD), has a height of 124 cm (−2.4 SD), and an OFC of 51 cm (−1.1 SD). Scoliosis has appeared. He can ride a bicycle and swim several meters. He tells his mother what happens at school, reads kanji (which children at his age learn), and likes proverbs. He can do arithmetic at a level comparable to that seen in the lower grade of an elementary school. Behavioral abnormalities have not been reported.

ARID1B-5 (Subject 12 [Tsurusaki et al., 2012]; Fig. 6u, v): He was born at 41 weeks of gestation. His birth weight was 2,264 g (−2.3 SD) and length was 43 cm (−3.7 SD). Motor development was moderately delayed: he walked by holding onto something at 2 years, and spoke only "no" at age 6 years. He had complex partial seizures at age 7 years. Scoliosis appeared and an infectious tumor at the sacral region was resected. He suffered from recurrent infections, gastric ulcers, and reflux esophagitis. At age 19 years, his weight is 40.7 kg (−2.3 SD) and height is 136 cm (−6.1 SD). He has mild mitral regurgitation. He walks independently and goes upstairs without support, but has severe ID and cannot speak meaningful words. He is irritable and hyperactive.

DISCUSSION

We have provided the clinical information of 21 patients with mutations in the components of the SWI/SNF complex. These patients were recruited with a clinical diagnosis of CSS, and 20 of them (except SMARCA4-7) were included in our previous study [Tsurusaki et al., 2012]. Combined with previous and recently published articles [Nagamani et al., 2009; Halgren et al., 2012; Hoyer et al., 2012; Michelson et al., 2012; Santen et al., 2012; van Houdt et al., 2012], *SMARCB1* mutations have been identified in

four patients, *SMARCA4* mutations in seven, *SMARCA2* mutations in 37, *SMARCE1* mutation in one, *ARID1A* mutations in three, and *ARID1B* mutations in 33 (Tables Ia–Ic). The mutations occurred de novo in all the patients whose parental samples were available.

The *SMARCB1* mutation "p.Lys364del." the only recurrent mutation in our series, has been found in three patients with strikingly similar manifestations. They all showed severe ID without speaking words, had typical coarse facial features (in early childhood: round face with thick and arched eyebrows, short nose with bulbous tip and anteverted nostrils, long philtrum, small mouth, and micro-retrognathia; later: broad nasal bridge without anteverted nostrils, broad philtrum, large tongue, and protruding jaw), significant hypoplasia of fifth fingers/toes and nail hypoplasia of fifth and other fingers/toes, sucking/feeding difficulties, and postnatal growth retardation. However, congenital malformations of internal organs were mild. The mutation "p.Lys364del" as well as the other missense mutation is supposed to exert dominant–negative or gain-of-function effects (excluding haploinsufficiency as a cause) [Tsurusaki et al., 2012].

Patients with *SMARCA4* mutations showed a wide range of ID and speech impairment. One patient with mild ID and one patient with moderate ID both had mild speech delay. In those with severe ID, one patient could speak several words and one patient could have a simple conversation. Autistic features/behavioral abnormalities including hyperactivity were observed in 4/5 (80%). Facial coarseness was minimal and everted upper lip vermilion with a short philtrum was characteristic in 4/7 (57%). Hypoplasia of fifth fingers/toes and nail hypoplasia of fifth and other fingers/toes were significant. Although sucking/feeding difficulties were noted in 6/7 (86%), postnatal growth was delayed in 4/7 (57%). One 3-bp in-frame deletion and six missense mutations identified in each patient could exert dominant–negative or gain-of-function effects [Tsurusaki et al., 2012].

Since heterozygous *SMARCA2* mutations in NCBRS were reported [van Houdt et al., 2012] after the submission of our previous work [Tsurusaki et al., 2012], the physical features of SMARCA2-1 (Subject 19 [Tsurusaki et al., 2012]) have been reassessed, and NCBRS is indeed appropriate as the clinical diagnosis. SMARCA2-1 had the main clinical features of NCBRS [Sousa et al., 2009]: prenatal growth retardation (29%), postnatal growth retardation (53%), moderate developmental delay (25%) with absent speech, seizures (63%), microcephaly (54%), sparse hair (97%), thick and anteverted alai nasi (89%), a broad philtrum (86%), a large mouth (94%), a thick lower lip vermilion (89%), prominent interphalangeal joints (80%), and prominent distal phalanges (60%; % values in parentheses indicate frequencies in *SMARCA2*-positive NCBRS patients [van Houdt et al., 2012]). Furthermore, hypoplastic fifth fingers/toes or fingernails/toenails have not been noted. van Houdt et al. [2012] speculated that the *SMARCA2* mutations identified in NCBRS patients would act in a dominant–negative or gain-of-function manner because of: the lack of NCBRS phenotypes in the 9p distal monosomy syndrome with deletions encompassing *SMARCA2*; absent major developmental abnormalities in mice lacking functional Smarca2; the lack of truncating *SMARCA2* mutations found in their series. SMARCA2-1 has a 55-kb intragenic deletion of *SMARCA2* resulting in the skipping of exons 20–27 [Tsurusaki et al., 2012], which overlaps the mutation-clustering region (exons 15–25) of *SMARCA2* found in NCBRS patients. Furthermore, the deletion of exons 20–27 results in in-frame deletion, which was confirmed by reverse transcription-polymerase chain reaction of the patient's lymphoblastoid cells (data not shown). Thus, abnormal SMARCA2 in this patient lacking one part of the DNA-dependent ATPase domain is suggested to cause abnormal functions.

SMARCE1-1, the only one with an *SMARCE1* mutation, showed severe ID without speaking words and significant hypoplasia of fifth fingers/toes and nail hypoplasia of fifth and other fingers/toes, whereas facial appearances were not typically coarse. Evaluation of more patients with *SMARCE1* mutations would be necessary to ascertain whether and how *SMARCE1* mutations can cause CSS-related phenotypes.

ARID1A mutations were associated with the severest phenotypes. All three patients showed severe ID without speaking words. They had severe physical complications requiring intensive treatment and surgery and which lead to early deaths in two subjects. Considering that the mutations included one frameshift mutation and two nonsense mutations, the haploinsufficiency of *ARID1A* would cause these phenotypes. The mutated transcripts from one of the nonsense mutations (p.Gln920*) were found to be subject to nonsense-mediated decay (NMD) [Tsurusaki et al., 2012].

ARID1B mutations have been associated with CSS in 11 patients [Santen et al., 2012; Tsurusaki et al., 2012] and syndromic ID in 22 [Nagamani et al., 2009; Halgren et al., 2012; Hoyer et al., 2012; Michelson et al., 2012]. Developmental delay/ID was severe in 12/25 (48%), moderate in 11/25 (44%), and mild in 2/25 (8%). Speech impairment was profound (no words) in 14/31 (45%), severe (several words) in 11/31 (35%), moderate (sentences) in 4/31 (13%), and mild in 2/31 (6%). Ten patients were reported to have autistic features/behavioral abnormalities including hyperactivity and impulsiveness. Agenesis or hypoplasia of the corpus callosum with or without colpocephaly was detected in 13/24 (54%). Facial coarseness was not significant and thin upper lip vermilion with a long or broad philtrum was characteristic. Hypoplasia of fifth digits/nails was mild or limited to toes or fingers. Although sucking/feeding difficulties were noted frequently (4/5 in our series), postnatal growth was delayed in 13/31 (42%). Considering that the mutations included seven nonsense mutations, seven frameshift mutations, 17 deletions (0.2–14.5 Mb), one translocation and one duplication of exons 4 and 5, the haploinsufficiency of *ARID1B* would cause the phenotypes. The mutated transcripts forming the mutations in ARID1B-1 (Subject 1 [Tsurusaki et al., 2012]; p.Ile560Glyfs*89) and ARID1B-3 (Subject 23 [Tsurusaki et al., 2012]; p.Arg1102*) were found to be subject to NMD, whereas the transcript from the mutated allele in ARID1B-4 (Subject 10 [Tsurusaki et al., 2012]; p.Asp1878Metfs*96), creating a premature stop codon in the last exon, escaped from NMD [Tsurusaki et al., 2012].

The most phenotypically similar condition to CSS is NCBRS [Schrier et al., 2012] and vice versa [Sousa et al., 2009]. Exome sequencing has proved the mutations in the genes comprising the SWI/SNF complex: *SMARCB1*, *SMARCA4*, *SMARCE1*, *ARID1A*, and *ARID1B* in CSS [Santen et al., 2012; Tsurusaki et al., 2012]; *SMARCA2* in NCBRS [Tsurusaki et al., 2012; van Houdt et al., 2012]. Interestingly, prominent interphalangeal joints and

prominent distal phalanges (i.e., the main features distinguishing NBS from CSS) were observed in a considerable number of patients (especially in older ones) in our series: prominent interphalangeal joints in 1/3 patients (21 years old) with an *SMARCB1* mutation, in 2/7 (16, 20 years) with *SMARCA4* mutations, in 2/5 (11, 19 years) with *ARID1B* mutations; prominent distal phalanges in 2/3 (7, 21 years) with an *SMARCB1* mutation, in 5/7 (4, 9, 11, 16, 20 years) with *SMARCA4* mutations, in 1/3 (10 years) with an *ARID1A* mutation, in 3/5 (7, 11, 13 years) with *ARID1B* mutations. Furthermore, array-based screening of patients with syndromic ID has demonstrated that *ARID1B* would be an important causative gene [Nagamani et al., 2009; Halgren et al., 2012; Hoyer et al., 2012; Michelson et al., 2012]. Clinical information about facial and digital features in those with *ARID1B*-related syndromic ID is limited, so whether they show the CSS phenotype is not known. With regard to patients with mutations in the components of the SWI/SNF complex in general, developmental delay/ID was a cardinal feature: severe in 49/77 (64%), moderate in 22/77 (29%), and mild in 6/77 (8%). Speech impairment was also observed in all subjects and was usually more severe than intellectual status: no words in 39/60 (65%), severe (several words) in 12/60 (20%), moderate (sentences, simple conversation) in 5/60 (8%), and mild in 4/60 (7%). Agenesis or hypoplasia of the corpus callosum was common (noted in 19/32 (59%)). Hypoplastic/absent fifth finger/toe as well as hypoplastic/absent fifth fingernail/toenail, which have been heavily emphasized in previous clinical descriptions of patients with CSS, are still considered to be physical hallmarks, observed in all but SMARCA-2 (Subject 19 [Tsurusaki et al., 2012]) in our series. Careful clinical investigation including observation of toes and toenails is crucial to detect these patients, because some of them do not have hypoplastic fifth finger(nail) but only have hypoplastic fifth toe(nail).

In conclusion, mutations in the components of the SWI/SNF complex are associated with syndromic developmental delay/ID that predominantly affect speech, and which are frequently accompanied by agenesis or hypoplasia of the corpus callosum. Mutations in *SMARCB1* can cause "classical" CSS with typical facial coarseness, significant digital/nail hypoplasia, severe ID impairment, and profound speech impairment. Mutations in *SMARCA4* can cause CSS without typical facial coarseness and with significant digital/nail hypoplasia and variable severities of ID and speech impairment. Mutations in *SMARCA2* can cause NBS. Mutations in *SMARCE1* can cause CSS without typical facial coarseness and with significant digital/nail hypoplasia, severe ID impairment, and profound speech impairment. Mutations in *ARID1A* can cause the severest type of CSS, with severe ID impairment, profound speech impairment, and serious physical complications. Mutations in *ARID1B* can cause CSS without typical facial coarseness and with mild digital/nail hypoplasia, variable severities of ID impairment, and speech impairment or cause syndromic ID. Considering practical clinical approaches such as rehabilitation focusing on communicative skills besides speech and future gene-based treatment [Gray, 2013], pathway-based "lumping" of these conditions "SWI/SNF-related ID syndromes" might be useful, whereas feature-based "splitting" is surely important in more careful management of patients with each condition. Exome sequencing could be a powerful tool to establish such a reclassification of disorders by uniting independently observed (but clinically similar) conditions such as oral-facial-digital syndrome type 1, Simpson–Golabi–Behmel syndrome, type 2, and Joubert syndrome-10 [Tsurusaki et al., 2013].

ACKNOWLEDGMENTS

We are grateful to all the patients and their families who participated in this study. We are also thankful to Professor Hennekam (Academic Medical Center, University of Amsterdam, Amsterdam, the Netherlands) for clinical assessment of SMARCA2-1 and meaningful suggestions. This work was supported by Research Grants from the Ministry of Health, Labour and Welfare (T.K., N.O., H.O, H.S., N.M., and N.M.); the Japan Science and Technology Agency (N.M.); the Strategic Research Program for Brain Sciences (N.M.); a Grant-in-Aid for Scientific Research on Innovative Areas (Transcription cycle) from the Ministry of Education, Culture, Sports, Science and Technology of Japan (N.M.); a Grant-in-Aid for Scientific Research from the Japan Society for the Promotion of Science (N.M.); a Grant-in-Aid for Young Scientists from the Japan Society for the Promotion of Science (H.S. and N.M.); a Grant for 2011 Strategic Research Promotion of Yokohama City University (N.M.); and Research Grants from the Japan Epilepsy Research Foundation (H.S.) and the Takeda Science Foundation (N.M. and N.M.).

REFERENCES

Coffin GS, Siris E. 1970. Mental retardation with absent fifth fingernail and terminal phalanx. Am J Dis Child 119:433–439.

Devy P, Baraitser M. 1991. Coffin–Siris syndrome. J Med Genet 28:338–341.

Fleck BJ, Pandya A, Vanner L, Kerkering K, Bodurtha J. 2001. Coffin–Siris syndrome: Review and presentation of new cases from a questionnaire study. Am J Med Genet 68:136–142.

Gray SJ. 2013. Gene therapy and neurodevelopmental disorders. Neuropharmacology 99:1–7.

Halgren C, Kjaergaard S, Bak M, Hansen C, El-Schich Z, Anderson C, Henriksen K, Hjalgrim H, Kirchhoff M, Bijlsma E, Nielsen M, den Hollander N, Ruivenkamp C, Isidor B, Le Caignec C, Zannolli R, Mucciolo M, Renieri A, Mari F, Anderlid BM, Andrieux J, Dieux A, Tommerup N, Bache I. 2012. Corpus callosum abnormalities, intellectual disability, speech impairment, and autism in patients with haploinsufficiency of *ARID1B*. Clin Genet 82:248–255.

Hoyer J, Ekici AB, Endele S, Popp B, Zweier C, Wiesener A, Wohlleber E, Dufke A, Rossier E, Petsch C, Zweier M, Göhring I, Zink AM, Rappold G, Schröck E, Wieczorek D, Riess O, Engels H, Rauch A, Reis A. 2012. Haploinsufficiency of *ARID1B*, a member of the SWI/SNF-a chromatin-remodeling complex, is a frequent cause of intellectual disability. Am J Hum Genet 90:565–572.

Michelson M, Ben-Sasson A, Vinkler C, Leshinsky-Silver E, Netzer I, Frumkin A, Kivity S, Lerman-Sagie T, Lev D. 2012. Delineation of the interstitial 6q25 microdeletion syndrome: Refinement of the critical causative region. Am J Med Genet Part A 158A:1395–1399.

Nagamani SC, Erez A, Eng C, Ou Z, Chinault C, Workman L, Coldwell J, Stankiewicz P, Patel A, Lupski JR, Cheung SW. 2009. Interstitial deletion of 6q25.2-q25.3: A novel microdeletion syndrome associated with microcephaly, developmental delay, dysmorphic features and hearing loss. Eur J Hum Genet 17:573–581.

Nicolaides P, Baraitser M. 1993. An unusual syndrome with mental retardation and sparse hair. Clin Dysmorphol 2:360–364.

Santen GW, Aten E, Sun Y, Almomani R, Gilissen C, Nielsen M, Kant SG, Snoeck IN, Peeters EA, Hilhorst-Hofstee Y, Wessels MW, den Hollander NS, Ruivenkamp CA, van Ommen GJ, Breuning MH, den Dunnen JT, van Haeringen A, Kriek M. 2012. Mutations in SWI/SNF chromatin remodeling complex gene *ARID1B* cause Coffin–Siris syndrome. Nat Genet 44:379–380.

Schrier SA, Bodurtha JN, Burton B, Chudley AE, Chiong MA, D'avanzo MG, Lynch SA, Musio A, Nyazov DM, Sanchez-Lara PA, Shalev SA, Deardorff MA. 2012. The Coffin–Siris syndrome: A proposed diagnostic approach and assessment of 15 overlapping cases. Am J Med Genet Part A 158A:1865–1876.

Sousa SB, Abdul-Rahman OA, Bottani A, Cormier-Daire V, Fryer A, Gillessen-Kaesbach G, Horn D, Josifova D, Kuechler A, Lees M, MacDermot K, Magee A, Morice-Picard F, Rosser E, Sarkar A, Shannon N, Stolte-Dijkstra I, Verloes A, Wakeling E, Wilson L, Hennekam RC. 2009. Nicolaides–Baraitser syndrome: Delineation of the phenotype. Am J Med Genet Part A 149A:1628–1640.

Tsurusaki Y, Okamoto N, Ohashi H, Kosho T, Imai Y, Hibi-Ko Y, Kaname T, Naritomi K, Kawame H, Wakui K, Fukushima Y, Homma T, Kato M, Hiraki Y, Yamagata T, Yano S, Mizuno S, Sakazume S, Ishii T, Nagai T, Shiina M, Ogata K, Ohta T, Niikawa N, Miyatake S, Okada I, Mizuguchi T, Doi H, Saitsu H, Miyake N, Matsumoto N. 2012. Mutations affecting components of the SWI/SNF complex cause Coffin–Siris syndrome. Nat Genet 44:376–378.

Tsurusaki Y, Kosho T, Hatasaki K, Narumi Y, Wakui K, Fukushima Y, Doi H, Saitsu H, Miyake N, Matsumoto N. 2013. Exome sequencing in a family with an X-linked lethal malformation syndrome: Clinical consequences of hemizygous truncating OFD1 mutations in male patients. Clin Genet 83:135–144.

van Houdt JK, Nowakowska BA, Sousa SB, van Schaik BD, Seuntjens E, Avonce N, Sifrim A, Abdul-Rahman OA, van den Boogaard MJ, Bottani A, Castori M, Cormier-Daire V, Deardorff MA, Filges I, Fryer A, Fryns JP, Gana S, Garavelli L, Gillessen-Kaesbach G, Hall BD, Horn D, Huylebroeck D, Klapecki J, Krajewska-Walasek M, Kuechler A, Lines MA, Maas S, Macdermot KD, McKee S, Magee A, de Man SA, Moreau Y, Morice-Picard F, Obersztyn E, Pilch J, Rosser E, Shannon N, Stolte-Dijkstra I, van Dijck P, Vilain C, Vogels A, Wakeling E, Wieczorek D, Wilson L, Zuffardi O, van Kampen AH, Devriendt K, Hennekam R, Vermeesch JR. 2012. Heterozygous missense mutations in *SMARCA2* cause Nicolaides–Baraitser syndrome. Nat Genet 44:445–449.

CLINICAL GENETICS An International Journal of Genetics, Molecular and Personalized Medicine

Clin Genet 2011: 80: 293–296
Printed in Singapore. All rights reserved

CLINICAL GENETICS
doi: 10.1111/j.1399-0004.2011.01644.x

Letter to the Editor

A novel homozygous mutation of *DARS2* may cause a severe LBSL variant

To the Editor:

Leukoencephalopathy with brain stem and spinal cord involvement, and lactate elevation (LBSL, MIM #611105) is an autosomal recessive disorder with an early childhood-to-adolescence onset. In 2003, van der Knaap et al. originally described LBSL, which is characterized by slowly progressive pyramidal, cerebellar, and dorsal column dysfunction with increased white matter lactate levels in magnetic resonance (MR) spectroscopy (1). Since the first discovery that LBSL is caused by mutations of the *DARS2* gene-encoding mitochondrial aspartyl-tRNA synthetase (MtAspRS) (2), *DARS2* mutations have been found in all the patients described (2–5), but none of them showed a homozygous mutation (all are compound heterozygotes), suggesting that the activity of mutant MtAspRS homodimers may be incompatible with human life (2, 5). Here, we describe, for the first time, a consanguineous family with a homozygous *DARS2* mutation.

Materials and methods

We analyzed a consanguineous family including three affected children diagnosed with leukoencephalopathy (Fig. 1a and Table 1). The proband (II-2) developed truncal ataxic gait at 3 years old. Her affected sister (II-3) and brother (II-4) also showed truncal ataxia at 6 and 11 months, respectively. All cases were presented with horizontal nystagmus, slurring speech, ataxic gait, muscle tonus abnormality, hypo- or hyperreflexia, and tremor as well as mental retardation. II-2 at age 21 years could slowly speak one or two words. Peripheral muscles atrophy, weakness and joints contractures in extremities, loss of deep tendons reflex and disturbed deep sensation were noted. II-3 and II-4 died of pneumonia at age 8 years and respiratory failure at age 2 years, respectively. Although there were differences in MR imaging characteristics from classical LBSL, there were also striking similarities. In our patients, the involvement of the cerebral and cerebellar white matter was more diffused and severe than in classical LBSL, but the affected brain stem and spinal cord tracts were the same (Fig. 1b and Table 1).

Linkage analysis and direct sequencing of *DARS2* were performed as previously reported (6). Immunoblotting was carried out using antihuman DARS2 antibody (ab69336, Abcam, Cambridge, UK) and anti-cytochrome *c* oxidase (COX) IV antibody (ab16056, Abcam).

Results

Homozygosity mapping of this consanguineous family revealed the largest 8.5 Mb homozygous region at chromosome 1q25.1 with the maximum LOD score of 1.329. Five additional microsatellite markers showed the consistent result (Fig. 1a). Within this region, *DARS2* gene was highlighted as the primary target as it was causative for the LBSL. We found that all affected children possessed homozygous, and parents and an unaffected sib had the heterozygous intronic change at 22 base pairs upstream of exon 3 (c.228-22T>A), respectively. This change was not observed in 395 controls. We examined its mutational effect by reverse transcriptase-polymerase chain reaction (RT-PCR) using mRNA of lymphoblastoid cell lines (LCLs) derived from the proband, her father (a carrier) and a normal control. A shorter PCR fragment which lacked the entire exon 3 was confirmed by sequencing (Fig. 1c,d). Furthermore, wild-type *DARS2* mRNA and MtAspRS protein were significantly decreased in proband's LCL (Fig. 1e,f). Other genes within the 1q25.1 region have not been checked.

Discussion

We found a novel homozygous mutation of *DARS2* in a diffuse leukoencephalopathy, which may be an LBSL variant. This change resulted in the decrease of normal protein level and may have contributed to this disease. Two possibilities for the increased severity are considered: (i) a

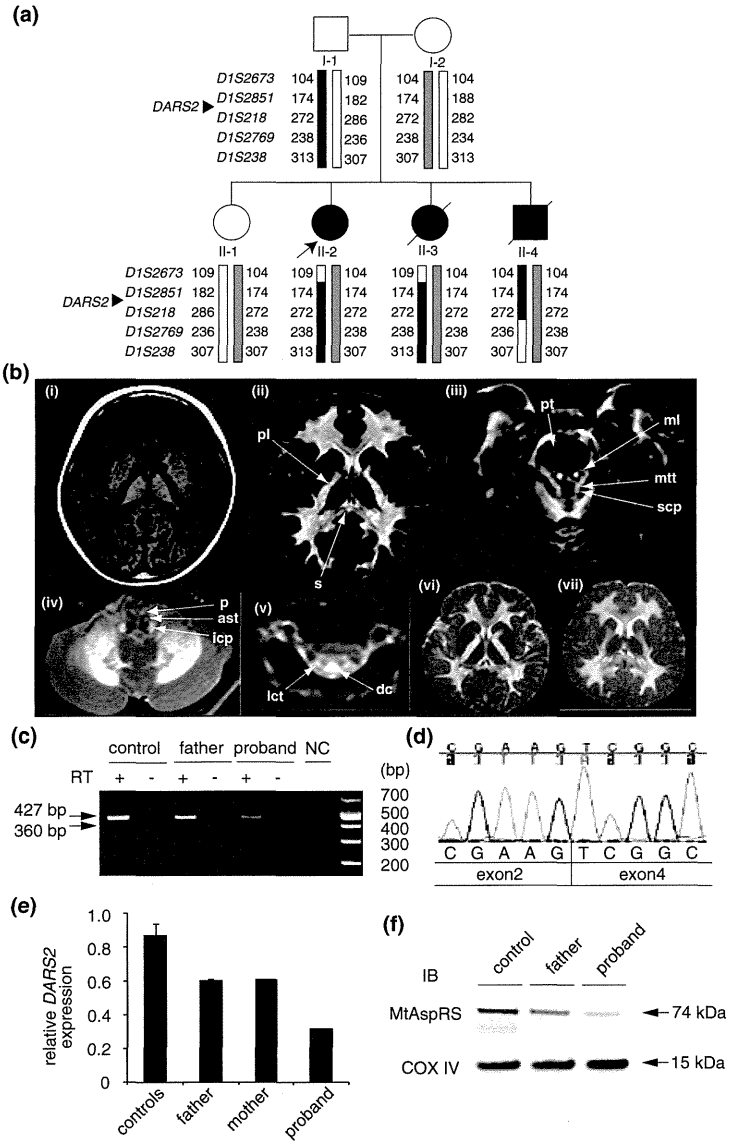

Fig. 1. Identification of a homozygous *DARS2* mutation causing abnormal splicing. (**a**) Haplotype analysis of the family. The black and gray bars represent disease alleles. The *DARS2* gene is located in between *D1S2851* and *D1S218*. (**b**) Magnetic resonance (MR) images of central nervous system in the proband (II-2) at 5 years (i–v), II-3 at 5 years (vi) and II-4 at 1 year and 4 months of age (vii). T_1-weighted (i) and T_2-weighted (T_2) (ii) images of cerebrum. The cerebral white matter was diffusely and severely affected, while the cerebral white matter involvement is less severe and more limited in extent in leukoencephalopathy with brain stem and spinal cord involvement, and lactate elevation with sparing of the U-fibers. Inhomogeneous signal abnormalities were observed in the posterior limb (pl) of the internal capsule and the splenium (s) of the corpus callosum. (iii) T_2 image at the level of the pons. The abnormal high-intensity signals were observed in pyramidal tracts (pt), medial lemniscus (ml), mesencephalic trigeminal tracts (mtt) and superior cerebellar peduncles (scp). (iv) T_2 image at the level of medulla. The pyramids (p), anterior spinocerebellar tracts (ast) and inferior cerebellar peduncles (icp) were affected. (v) T_2 image at the level of the cervical spinal cord. The dorsal columns (dc) and lateral corticospinal tracts (lct) showed abnormal signals. II-3 (vi) and II-4 (vii) showed the similar MR images as the proband. (**c**) RT-PCR using cDNA extracted from LCLs of a normal control, father and the proband. A shorter fragment (360 bp) in addition to a normal product (427 bp) was seen in father and the proband. (**d**) Electropherogram of the shorter fragment showing skipping of exon 3. (**e**) Relative expression of wild-type *DARS2* mRNA compared to β-actin mRNA in LCLs were determined by quantitative real-time RT-PCR using TaqMan Gene Expression Assays (Applied Biosystems, Bedford, MA). The relative *DARS2* expression was analyzed using TaqMan Probe (Applied Biosystems, Hs01016215_m1 for *DARS2* and 4326135E for β-actin as a control). Levels are shown for three controls, parents and the proband based on the calibration curve method using an independent control. Average of duplicated experiments is shown as black bars with the standard error of means. The significant decreased expression of *DARS2* mRNA in the proband was recognized compared to that in three controls ($p < 0.001$, one-way analysis of variance with Bonferroni's multiple comparison test). (**f**) Mitochondrial aspartyl-tRNA synthetase (MtAspRS) protein is expressed in normal control and father as a carrier (fainter), but only weakly recognized in the proband. Cyclooxygenase IV was used as a loading control for the mitochondrial fraction.

Table 1. MRI criteria for LBSL and clinical features of patients

Diagnostic criteria	Case 1	Case 2	Case 3
Major criteria			
Signal abnormalities in			
1. the cerebral white matter, either inhomogeneous and spotty or homogeneous and confluent, sparing the U-fibers	±[a]	±[a]	±[a]
2. the dorsal columns and lateral corticospinal tracts of the spinal cord. (visualization of such abnormalities in the cervical spinal cord suffices)	+	n.e.[b]	n.e.
3. the pyramids of the medulla oblongata	+	+	+
Supportive criteria			
Signal abnormalities in			
1. the splenium of the corpus callosum	+	+	+
2. the posterior limb of the internal capsule	+	+	+
3. the medial lemniscus in the brain stem	+	+	+
4. the superior cerebellar peduncles	+	+	+
5. the inferior cerebellar peduncles	+	n.e.	n.e.
6. the intraparenchymal part of the trigeminal nerve	−	n.e.	n.e.
7. the mesencephalic trigeminal tracts	+	n.e.	n.e.
8. the anterior spinocerebellar tracts in the medulla	+	n.e.	n.e.
9. the cerebellar white matter with subcortical preponderance	−	−	−
Elevated lactate of abnormal cerebral white matter (MRS)	+	Not performed	+

LBSL, leukoencephalopathy with brain stem and spinal cord involvement, and lactate elevation; MRI, magnetic resonance imaging; MRS, magnetic resonance spectroscopy.
[a]Homogeneous and confluent abnormal high intensity was observed, but sparing the U-fibers was unclear because of the strenuous pathological change in the white matter.
[b]n.e., not evaluated as MRI images were unavailable.

(unidentified) modifier effect in the family and (ii) this particular homozygous mutation caused the severe variant because of the substantially decreased normal protein level, although it is not full proof.

Interestingly, affected allele frequency varies, depending on the ethnicity. For example, *DARS2* mutations are the most common causes of childhood onset leukoencephalopathy in Finland, because of high carrier frequency (1:95 for the c.228-20_21delTTinsC and 1:380 for the c.492+2T>C) (4). Thus, further analysis of the *DARS2* gene in LBSL as well as childhood-to-adult onset leukoencephalopathy of unknown cause in different populations would lead us to fully understand phenotypes of the *DARS2* abnormalities.

Acknowledgements

We thank all the patients and their families for participating in this work. We also thank Ms. Y. Yamashita for her technical assistance. This work was supported by Research Grants from the Ministry of Health, Labour and Welfare (N. M., H. S., and N. M.), the Japan Science and Technology Agency (N. M.), Grant-in-Aid for Scientific Research from Japan Society for the Promotion of Science (N. M.), Grant-in-Aid for Young Scientist from Japan Society for the Promotion of Science (N. M. and H. S.), Grant for 2010 Strategic Research Promotion of Yokohama City University (N. M.), Research Grants from the Japan Epilepsy Research Foundation (H. S.), and Research Grant from Naito Foundation (N. M.), the Takeda Science Foundation (N. M. and N. M.), the Yokohama Foundation for Advancement of Medical Science (N. M.), and the Hayashi Memorial Foundation for Female Natural Scientists (N. M.).

N Miyake[a]
S Yamashita[b]
K Kurosawa[c]
S Miyatake[a]
Y Tsurusaki[a]
H Doi[a]
H Saitsu[a]
N Matsumoto[a]
[a]Department of Human Genetics, Yokohama City University Graduate School of Medicine, Yokohama, Japan,
[b]Division of Child Neurology, and
[c]Division of Medical Genetics, Kanagawa Children's Medical Center, Yokohama, Japan

References

1. van der Knaap MS, van der Voorn P, Barkhof F et al. A new leukoencephalopathy with brainstem and spinal cord involvement and high lactate. Ann Neurol 2003: 53: 252–258.
2. Scheper GC, van der Klok T, van Andel RJ et al. Mitochondrial aspartyl-tRNA synthetase deficiency causes leukoencephalopathy with brain stem and spinal cord involvement and lactate elevation. Nat Genet 2007: 39: 534–539.
3. Uluc K, Baskan O, Yildirim KA et al. Leukoencephalopathy with brain stem and spinal cord involvement and high lactate:

a genetically proven case with distinct MRI findings. J Neurol Sci 2008: 273: 118–122.
4. Isohanni P, Linnankivi T, Buzkova J et al. *DARS2* mutations in mitochondrial leucoencephalopathy and multiple sclerosis. J Med Genet 2010: 47: 66–70.
5. Lin J, Faria EC, Da Rocha AJ et al. Leukoencephalopathy with brainstem and spinal cord involvement and normal lactate: a new mutation in the *DARS2* gene. J Child Neurol 2010: 25: 1425–1428.
6. Miyake N, Kosho T, Mizumoto S et al. Loss-of-function mutations of *CHST14* in a new type of Ehlers-Danlos syndrome. Hum Mutat 2010: 31: 966–974.

Correspondence:
Noriko Miyake, MD, PhD
Department of Human Genetics
Yokohama City University Graduate School of Medicine
3-9 Fukuura
Kanazawa-ku
236-0004 Yokohama
Japan
Tel.: +81 45 787 2606
Fax: +81 45 786 5219
e-mail: nmiyake@yokohama-cu.ac.jp

ORIGINAL ARTICLE

PAPSS2 mutations cause autosomal recessive brachyolmia

Noriko Miyake,[1] Nursel H Elcioglu,[2] Aritoshi Iida,[3] Pinar Isguven,[4] Jin Dai,[3] Nobuyuki Murakami,[5] Kazuyuki Takamura,[6] Tae-Joon Cho,[7] Ok-Hwa Kim,[8] Tomonobu Hasegawa,[9] Toshiro Nagai,[5] Hirofumi Ohashi,[10] Gen Nishimura,[11] Naomichi Matsumoto,[1] Shiro Ikegawa[3]

[1]Department of Human Genetics, Yokohama City University Graduate School of Medicine, Yokohama, Japan
[2]Department of Pediatric Genetics, Marmara University Pendik Hospital, Istanbul, Turkey
[3]Laboratory for Bone and Joint Diseases, Center for Genomic Medicine, RIKEN, Tokyo, Japan
[4]Department of Pediatrics and Pediatric Endocrinology, Medeniyet University Goztepe Hospital, Istanbul, Turkey
[5]Department of Pediatrics, Dokkyo Medical University Koshigaya Hospital, Koshigaya, Japan
[6]Department of Orthopaedic Surgery, Fukuoka Children's Hospital, Fukuoka, Japan
[7]Division of Pediatric Orthopaedics, Seoul National University Children's Hospital, Seoul, Korea
[8]Department of Radiology, Ajou University Hospital, Suwon, Korea
[9]Department of Pediatrics, Keio University School of Medicine, Tokyo, Japan
[10]Division of Medical Genetics, Saitama Children's Medical Center, Saitama, Japan
[11]Department of Pediatric Imaging, Tokyo Metropolitan Children's Medical Center, Futyu, Japan

Correspondence to
Noriko Miyake, Department of Human Genetics, Yokohama City University Graduate School of Medicine, 3-9, Fukuura, Kanazawa-ku, Yokohama 236-0004, Japan; nmiyake@yokohama-cu.ac.jp or Shiro Ikegawa, Laboratory of Bone and Joint Diseases, Center for Genomic Medicine, RIKEN 4-6-1 Shirokanedai, Minato-ku, Tokyo 108-8639, Japan; sikegawa@ims.u-tokyo.ac.jp

NM, NHE and AI contributed equally to this work.

Received 8 May 2012
Revised 8 June 2012
Accepted 10 June 2012

ABSTRACT

Background Brachyolmia is a heterogeneous group of skeletal dysplasias that primarily affects the spine. Clinical and genetic heterogeneity have been reported; at least three types of brachyolmia are known. *TRPV4* mutations have been identified in an autosomal dominant form of brachyolmia; however, disease genes for autosomal recessive (AR) forms remain totally unknown. We conducted a study on a Turkish family with an AR brachyolmia, with the aim of identifying a disease gene for AR brachyolmia.

Methods and results We examined three affected individuals of the family using exon capture followed by next generation sequencing and identified its disease gene, *PAPSS2* (phosphoadenosine-phosphosulfate synthetase 2). The patients had a homozygous loss of function mutation, c.337_338insG (p.A113GfsX18). We further examined three patients with similar brachyolmia phenotypes (two Japanese and a Korean) and also identified loss of function mutations in *PAPSS2*; one patient was homozygous for IVS3+2delT, and the other two were compound heterozygotes for c.616-634del19 (p.V206SfsX9) and c.1309-1310delAG (p.R437GfsX19), and c.480_481insCGTA (p.K161RfsX6) and c.661delA (p.I221SfsX40), respectively. The six patients had short-trunk short stature that became conspicuous during childhood with normal intelligence and facies. Their radiographic features included rectangular vertebral bodies with irregular endplates and narrow intervertebral discs, precocious calcification of rib cartilages, short femoral neck, and mildly shortened metacarpals. Spinal changes were very similar among the six patients; however, epiphyseal and metaphyseal changes of the tubular bones were variable.

Conclusions We identified *PAPSS2* as the disease gene for an AR brachyolmia. *PAPSS2* mutations have produced a skeletal dysplasia family, with a gradation of phenotypes ranging from brachyolmia to spondylo-epi-metaphyseal dysplasia.

INTRODUCTION

Brachyolmia is a heterogeneous group of skeletal dysplasias that primarily affects the spine. The name comes from the Greek for 'short trunk'; patients with brachyolmia have short stature due to a short trunk.[1] Conceptually, skeletal lesions of brachyolmia are limited to the spine; however, it is generally thought that pure brachyolmia (spine-only dysplasia) does not exist and that metaphyseal and/or epiphyseal involvements may be minimal and scattered, but are always present along with spinal involvements in cases labelled brachyolmia.[2]

Clinical and genetic heterogeneity have been reported in brachyolmia. At least three relatively well defined types of brachyolmia are known: type 1 that includes the Hobaek (OMIM 271530) and Toledo (OMIM 271630) forms; type 2 (OMIM 613678) referred to as the Maroteaux type; and type 3 (OMIM 113500). The former two types are autosomal recessive (AR) traits, while the latter is an autosomal dominant trait. Type 1 is characterised by scoliosis, platyspondyly with rectangular and elongated vertebral bodies, overfaced pedicles, and irregular and narrow intervertebral spaces. The Toledo form is distinguished from the Hobaek form by the presence of corneal opacity and precocious calcification of the costal cartilage.[3 4] Type 2 is distinguished by rounded vertebral bodies, less overfaced pedicles, minor facial anomalies, and precocious calcification of the falx cerebri.[1] Type 3 is characterised by severe kyphoscoliosis and flattened, irregular cervical vertebrae. Heterozygous mutations in the *TRPV4* (transient receptor potential vanilloid 4) gene (OMIM 605427) have been identified in several patients with type 3, autosomal dominant brachyolmia;[5 6] however, disease genes for recessive forms of brachyolmia remain totally unknown.

To identify novel disease genes from a limited number of subjects, exome sequencing (exon capture followed by next generation sequencing) is a promising approach. This approach sometimes presents us with unusual and unexpected connection between genes and phenotypes, thereby opening a new window for biology and medicine. We experienced a family with an AR form of brachyolmia harbouring three affected individuals. By performing exome sequencing for the family, we have identified the disease gene for the recessive brachyolmia, *PAPSS2* (phosphoadenosine-phosphosulfate synthetase 2). The discovery was confirmed by identification of *PAPSS2* mutations in three sporadic patients with different ethnic backgrounds but similar brachyolmia phenotypes. All patients had loss of function mutations of *PAPSS2* in both chromosomes.

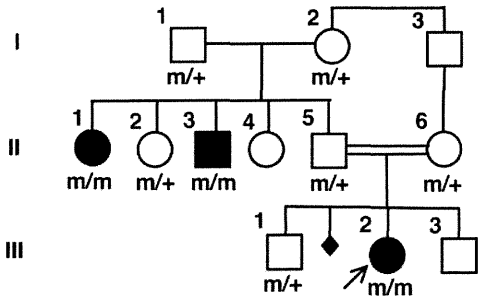

Figure 1 The pedigree of family 1 and co-segregation of the *PAPSS2* mutation (c.337_338insG) in the family. m: mutation allele, +: wild type allele.

MATERIALS AND METHODS

Subjects

P1-3 (family 1)

The proband (P1; III-2 in figure 1) was a Turkish girl referred to one of us (NHE) for genetic evaluation at the age of 8 years 4 months. She has been followed up for her spinal deformity and lumber pain elsewhere for 5 years. She was the result of a consanguineous (first cousin) marriage. A paternal uncle (P2; II-3 in figure 1) and aunt (P3; II-1 in figure 1) had the similar disease (table 1). The paternal grandparents originated from a small area and could be related. The inheritance of the disease was consistent with AR mode. Her birth length was 49 cm and weight 2800 g. She did not gain well after birth and was investigated for short stature at the age of 1 year. Her back deformity was noticed at around 3 years of age. On examination, she had short-trunk short stature. Her height was 109 cm (−3.2 SD), weight 29 kg (+0.38 SD) and head circumference 51 cm (−0.6 SD). She was mentally normal with no hearing or vision problems. She had widened wrists, bulbous proximal interphalangeal joints, clinodactyly of the fifth finger, and bowing deformity in her left lower leg. Serum DHEA-S (dehydroepiandrosterone-sulfate) was under the detection limit (<15.0 μg/dl).

Repeated skeletal surveys showed definite spondylodysplasia with minimal epiphyseal and metaphyseal changes, which was compatible with brachyolmia (table 1 and figure 2). Vertebral bodies were flat, particularly in thoracic spines. Endplates were irregular and intervertebral disc spaces were narrowed. The acetabular roof was horizontal. Femoral necks were slightly short. Metaphyses of the distal tibias had striation. Metacarpals were mildly shortened with mild metaphyseal changes. The bone age was advanced; 6 years 10 months at chronological age 5 years 8 months, and 10 years at chronological age 8 years 2 months (Greulich-Pyle method). MRIs and CTs showed no calcification of the falx cerebri.

At her last visit (10 years 4 months old), she had increasing back deformity and pain. Her height was 121 cm (−3.4 SD), arm span 119 cm, and sitting/standing height ratio was 0.53.

Table 1 Clinical and radiographic phenotypes of autosomal recessive brachyolmina harbouring *PAPSS2* mutation (in comparison to those in spondylo-epi-metaphyseal dysplasia Pakistani type)

Patient ID	P1	P2	P3	P4	P5	P6	
Family	Family 1						Patient reported by Noordam *et al*
Intra-family ID	III-2	II-3	II-1	Family 2	Family 3	Family 4	
Country of origin	Turkey			Japan	Japan	Korea	Turkey
Sex	Female	Male	Female	Female	Female	Male	Female
Age at first presentation	8 years 4 months	29 years	40 years	11 years 4 months	8 years 8 months	12 years 7 months	8 years
Birth length (cm)	49	NA	NA	46	47	50	NA
Birth weight (g)	2800	NA	NA	3340	2676	3100	NA
Consanguinity of the parents	+	Probably +	Probably +	(−)	(−)	(−)	(−)
Clinical feature							
Normal intelligence	+	+	+	+	+	+	NA
Normal facies	+	+	+	+	+	+	NA
Short-trunk short stature	+	+	+	+	+	+	+
Spinal deformity	Kyphosis	(−)	Kyphosis, lumbar scoliosis	Kyphosis	(−)	(−)	Lumbar scoliosis
Leg deformity	*Bil genu varum* and internal rotation	(−)	*Bil genu varum* and internal rotation	(−)	*Right genu* valgum	*Bil genu* varum	NA
Androgen excess sign	(−)	(−)	(−)	(−)	(−)	(−)	+
Radiographic feature							
Rectangular vertebra	+	+	+	+	+	+	+
Irregular endplate	+	+	+	+	+	+	+
Narrowed disc	+	+	+	+	+	+	+
Precocious calcification of costal cartilage	(−)	+	+	+	(−)	(−)	NA
Delayed ossification of hip and knee epiphyses	(−)	NA	NA	(−)	(−)	(−)	(−)
Early osteoarthritic change	(−)*	(−)	(−)	(−)	(−)*	(−)*	(−)*
Short femoral neck	+	+	+	+	+	+	+
Metaphyseal abnormality†	Dist tibia	Prox tibia	Prox tibia	(−)	(−)	Prox tibia	(−)
Mild brachymetacarpia	+	+	+	+	+	+	+
Advanced bone age	+	NA	NA	+	+	+	+

*May be too young to be evaluated.
†Other than short femoral neck and fingers.
Bil, bilateral; Dist, distal; NA, not available or assessed; Prox, proximal.

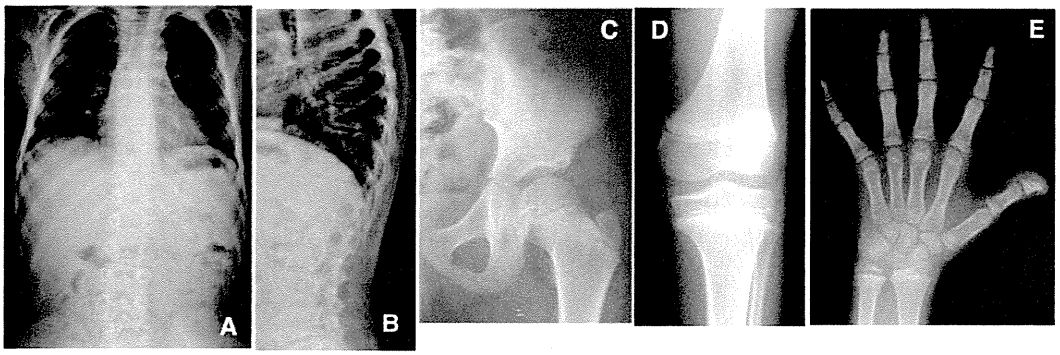

Figure 2 Radiographs of P1 (III-2 in family 1) at age 8.5 years. (A) Spine anteroposterior (AP). Mildly overfaced vertebra. (B) Lateral spine. Mild flattening of vertebral bodies and irregular endplates. (C) Left hip AP. Almost normal epiphysis. (D) Left knee AP. Epiphyseal and metaphyseal abnormalities are unremarkable. (E) Left hand AP. Metacarpals are mildly shortened with mild irregularity of the growth plates. Epiphyses of the distal radius and ulna show mild dysplasia. The bone age is advanced.

Breast development was Tanner 2–3, pubic hair Tanner 1. There had been no sign of androgen excess (acne, hirsutism, etc).

P4-6 (sporadic cases)

After we found *PAPSS2* mutations in family 1, we reviewed the patient registry of the Japanese Skeletal Dysplasia Consortium and found two Japanese patients (P4-5) and one Korean patient (P6) who had similar phenotypes to those of the Turkish family (table 1 and figure 3); all three were sporadic cases from normal, non-consanguineous parents and were *TRPV4* mutation negative.

DNA sample

Genomic DNA was extracted by standard procedures from peripheral blood of the patients and/or their family members after informed consent. The study was approved by the ethical committee of RIKEN, Yokohama City University, and participating institutions.

Exome sequencing

Three affected individuals of family 1 (II-1, II-3 and III-2) were analysed by whole exome sequencing as previously reported (see supplementary online table S1).[7 8] In brief, 3 μg of genomic DNA was sheared by Covaris S2 system (Covaris, Woburn, Massachusetts, USA) and processed using a SureSelect Human All Exon 50 Mb Kit (Agilent Technologies, Santa Clara, California, USA) according to the manufacturer's instructions. DNAs were captured by the kit and were sequenced by GAIIx (Illumina, San Diego, California, USA) with 108 pair-ends reads. Each sample was run in one lane. Image analysis and base calling were performed by sequence control software 2.9 and real time analysis 1.9 (Illumina), and CASAVA software V.1.8.1 (Illumina). The quality-controlled (path-filtered) reads were mapped to human genome reference hg19 with Mapping and Assembly with Qualities (MAQ, http://maq.sourceforge.net/) and NextGENe software V.2.00 (SoftGenetics, State College, Pennsylvania, USA). The variants from MAQ were annotated by SeattleSeq annotation 131 (http://snp.gs.washington.edu/SeattleSeqAnnotation131/).

Priority scheme

Variants were filtered by the following conditions using the script created by BITS (Tokyo, Japan): (1) variants only annotated on human autosomes and chromosome X; (2) variants not in dbSNP131, dbSNP134, the 1000 Genomes database (http://www.1000genomes.org/), and in-house exome data of normal Japanese controls (n=66); (3) variants that were non-synonymous and intronic changes (±20 bp from exon/intron boundaries) called in common by NextGENe and MAQ, and variants of insertion/deletion with a NextGENe score ≥10. The variant numbers in each category are shown in supplementary online table S1.

Sanger sequencing and evaluation of mutations

To confirm the sequence change identified in P1-3 by the exome sequencing, exon 3 of *PAPSS2* and its flanking intronic sequences (The GenBank reference sequence: NM_001015880) were amplified by PCR from genomic DNA. To examine *PAPSS2* mutation in P4-6, all exons of *PAPSS2* and its flanking intronic sequences were amplified by PCR from genomic DNA. Primer sequences and PCR conditions were as previously described.[9] PCR products were directly sequenced using ABI Prism automated sequencers 3730 (PE Biosystems, Foster City, CA, USA).

To evaluate the possibility of polymorphisms, identified sequence changes were genotyped in 93 ethnically matched controls using the invader assay coupled with PCR as described previously.[10] The sequence changes were evaluated by public databases including OMIM (http://www.ncbi.nlm.nih.gov/omim) and dbSNP (http://www.ncbi.nlm.nih.gov/projects/SNP/).

RESULTS

Exome sequencing

A total of 90 964 194 (II-1), 90 508 738 (II-3) and 90 223 680 (III-2) reads were mapped to the whole human genome in pairs by MAQ. Considering the consanguinity of the family, we focused on the same homozygous mutations shared by the three affected individuals. After filtering, a total of 37 homozygous variants remained as candidates (23 missense, 11 intronic, and three insertion changes) (see supplementary online table S1). Among them, one base pair insertion, c.337_338insG in exon 3 of *PAPSS2*, was highlighted because it is a causative gene for SEMD, Pakistani type (OMIM 612847), that has overlapping features with the phenotypes of the three patients.

The insertion sequence was confirmed by direct sequence of PCR products from genomic DNA. Direct sequencing of nine family members showed co-segregation of the mutation with the disease phenotype (figure 1). The insertion mutation was

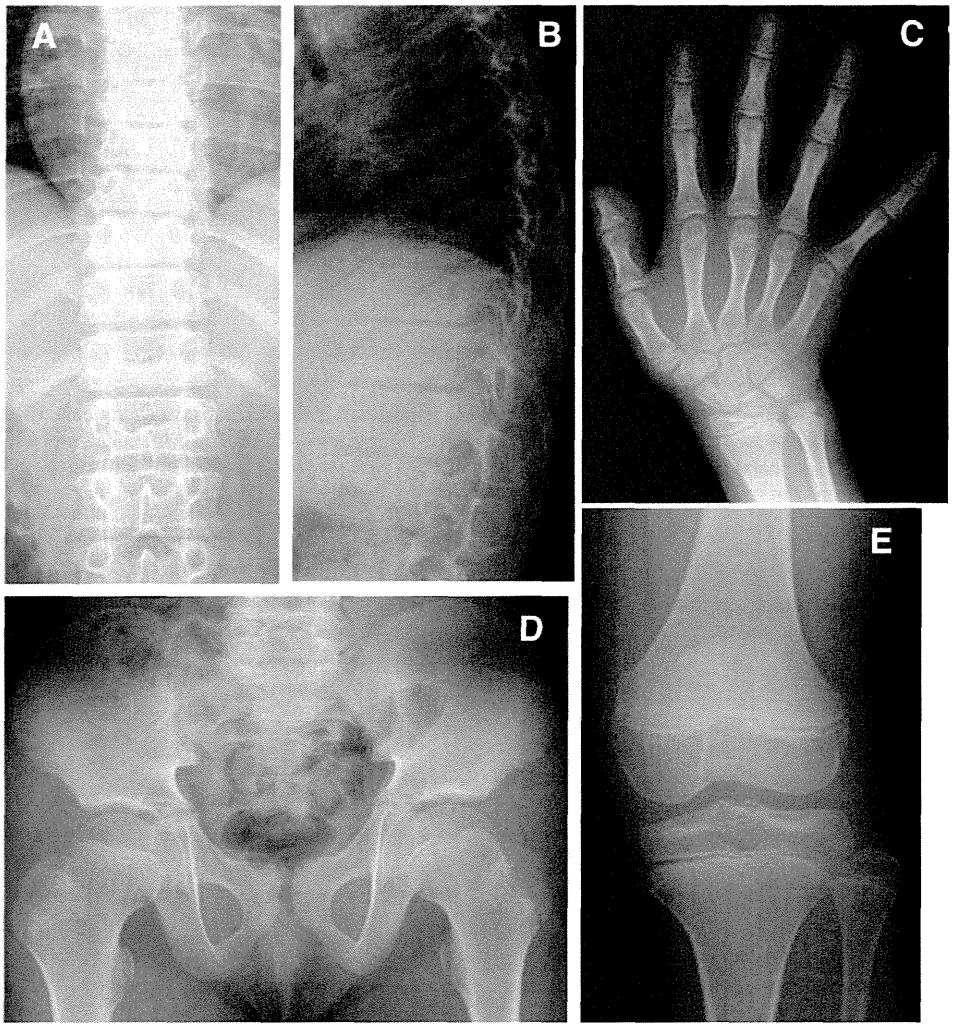

Figure 3 Radiographs of P5 at age 8 years 8 months. (A) Spine anteroposterior (AP). Platyspondyly. Over-faced pedicle is not so distinct. (B) Spine lateral. Flattened vertebral bodies and narrow disc spaces. (C) The right hand AP. Slightly short metacarpals. Phalanges are not so short. The bone age is advanced (12 years by the Greulich-Pyle method). (D) Pelvis AP. Short femoral neck and horizontal acetabulum. Proximal epiphyses are normal. (E) The right knee AP. Unremarkable changes. No fibula overgrowth.

predicted to create a premature stop codon (p.A113GfsX18), thereby most probably resulting in a null allele due to nonsense mutation mediated RNA decay (NMD).[11] The mutation was not found in the public mutation database and sequence variation database. Also, it was not found in 93 ethnically matched controls examined by Invader assay.[10]

Identification of *PAPSS2* mutations in sporadic cases

We screened for *PAPSS2* mutations in P4-6 by direct sequencing as previously described.[9] We found *PAPSS2* mutations in both chromosomes of all subjects (table 2). All mutations are predicted to create premature stop codons before the second last exon of the gene. Therefore, they are most likely to result in null alleles due to NMD. P5 was a homozygote, and P4 and P6 were heterozygotes for the mutations. Compound heterozygosity of the subjects was confirmed by sequencing of the parents' genomic DNA. All these mutations were not found in 93 ethnically matched controls examined by Invader assay[10] nor in public databases.

Phenotypes of the patients with *PAPSS2* mutations

Clinical features of our six patients were short-trunk short stature with short neck (table 1). The short stature was noticeable early in life, but not always at birth; it usually became definite after age 5–6 years. All patients had normal intelligence and facies. Corneal opacity was not found. Kyphosis and/or scoliosis were found in three subjects. Bone age was advanced in all (4/4) cases evaluated. No clinical sign of androgen excess was noted in all (6/6) patients and their family members. The main radiographic feature was pronounced flattening of spine (rectangular vertebral body), particularly in the thoracic spine, which accompanied irregular

Table 2 *PAPSS2* mutations in autosomal recessive brachyolmia

Family	Exon	Nucleotide change	Amino acid change
1	3	c.337_338insG (homozygous)	p.A113GfsX18
2	5	c.616-634del19	p.V206SfsX9
	11	c.1309-1310delAG	p.R437GfsX19
3	3	IVS3+2delT (homozygous)	p.L50SfsX2
4	4	c.480_481insCGTA	p.K161RfsX6
	6	c.661delA	p.I221SfsX40

The nucleotide changes are shown with respect to *PAPSS2* mRNA sequence (NM_001015880). The corresponding predicted amino acid changes are numbered from the initiating methionine residue. Exons are numbered sequentially 1–13.

endplates and narrow disc spaces. Mild shortening of the femoral neck and metacarpals were common features. The costal cartilages showed precocious calcification in the adult subjects (3/3). Epiphyseal and metaphyseal dysplasias were very mild, if present. From these features of spine predominant dysplasia, our patients can be diagnosed as having brachyolmia. Among known types of brachyolmias, characteristics of the Hobaek and Toledo types are mixed.[1 4]

DISCUSSION

PAPSS2 mutation has been reported to be responsible for two other overlapping, but distinct, phenotypes. The first is SEMD Pakistani type; Ahmad *et al*[12] described a large consanguineous Pakistani family with a distinct form of SEMD with autosomal inheritance. Its clinical features include short stature evident at birth, short and bowed lower limbs, mild brachydactyly, kyphoscoliosis, enlarged knee joints, and precocious osteoarthropathy. Radiographic features are platyspondyly with irregular endplates and narrowed joint spaces, delayed epiphyseal ossification at the hips and knees, diffuse early osteoarthritic changes primarily in the spine and hands, and mild brachydactyly. Metaphyseal abnormalities are seen predominantly in the hips and knees. This disease is differentiated from other forms of SEMD by its mild degree of metaphyseal involvement, type of brachydactyly, and the absence of loose joints or other clinical findings. A homozygous nonsense mutation of *PAPSS2* (S438X) is identified in all affected individuals in the family.[13] Many of the characteristics of SEMD Pakistani type, including enlarged joints with deformity, delayed epiphyseal ossification at the hips and knees, and precocious osteoarthritic changes of the large and small joints, are absent in our cases (table 1).

PAPSS2 mutations have also been found in a patient with a different phenotype, spondylodysplasia and premature pubarche.[9] A Turkish girl with premature pubarche, hyperandrogenic anovulation, short stature, and skeletal dysplasia showed a compound heterozygosity for a missense and a nonsense mutation in *PAPSS2*: the former was a 143C>G transversion resulting in a T48R substitution at a conserved residue in the adenosine 5-prime-phosphosulfate kinase domain, and the latter was a 985C>T transition resulting in R329X. Their functional assays revealed no detectable activity for R329X, and only minor residual activity for T48R (6% of the wild type activity). The mother who carried the R329X mutation had normal pubarche and menarche, but developed obesity, oligomenorrhoea, and hirsutism in her fourth decade, while the father who carried the T48R mutation showed normal growth and pubertal development. The skeletal changes in this patient are more similar to those of our cases than SEMD Pakistani type (table 1).

Among our patients, spinal changes were very similar, but epiphyseal and metaphyseal changes were considerably variable (table 1). P4 and P5, similar to the case reported by Noordam *et al*,[9] showed minimal epiphyseal and metaphyseal dysplasias. P6 had considerable epi-metaphyseal changes in the long bones of the lower extremities; they were more severe than those in family 1 (P1-3), but were far milder than those in SEMD Pakistani type. The differential diagnosis includes AR spondyloepiphyseal dysplasia tarda[14] because of late manifestation, AR inheritance, and relatively mild spondyloepiphyseal dysplasia with flat vertebral bodies with irregular endplates. In the disorder, overfaced vertebral bodies is absent and the capital femoral epiphyses are severely affected.[14]

In a form of autosomal dominant brachyolmia, heterozygous *TRPV4* mutation has been identified.[5 6] Notably, the *TRPV4* mutation presents a wide phenotypic gradation from brachyolmia at its most mild, through spondylometaphyseal dysplasia type Kozlowski, spondyloepiphyseal dysplasia type Maroteaux, and metatropic dysplasia, to parastremmatic dysplasia and fetal akinesia at its most severe.[5 15–17] *PAPSS2* mutations might also present a phenotype gradation from brachyolmia to spondylo-epiphyseal and spondylo-epimetaphyseal dysplasia like SEMD Pakistani type. Further investigation of *PAPSS2* mutations in brachyolmia and skeletal dysplasias with overlapping phenotypes to our cases as well as other cases with *PAPSS2* mutations[9 14] would provide further answers.

An additional supplementary table is published online only. To view this file please visit the journal online (http://jmg.bmj.com)

Acknowledgements We thank the patients and their family for their help to the study. We also thank the Japanese Skeletal Dysplasia Consortium.

Contributors NM performed the exome experiments, analysed the data, wrote the paper, and is guarantor. NE and PI collected family samples and evaluated their phenotypes. AI performed the sequence experiments, analysed the data, and wrote the paper. JD performed the experiments. NoM, KM, TC, OK, and TN collected samples and evaluated their clinical and radiographic phenotypes. TH and GN analysed the clinical data. HO collected and controlled the experimental samples. NaM performed the experiments and analysed the data. SI analysed the data, wrote the paper, and is also guarantor. All authors have critically revised the paper.

Funding This study is supported by research grants from the Ministry of Health, Labour and Welfare (23300101: S Ikegawa and N Matsumoto; 23300102: T Hasegawa; 23300201: S Ikegawa), by a Grant-in-Aid for Young Scientists from the Japan Society for the Promotion of Science (N Miyake), and by Research on intractable diseases, Health and Labour Sciences Research Grants, H23-Nanchi-Ippan-123 (S Ikegawa).

Patient consent Obtained.

Ethics approval This study was performed under the approval of the ethical committee of RIKEN, Yokohama City University, and participating institutions.

Provenance and peer review Not commissioned; externally peer reviewed.

Data sharing statement Additional unpublished data on mutation examination are available on request to researchers.

REFERENCES

1. **Shohat M,** Lachman R, Gruber HE, Rimoi DL. Brachyolmia: radiographic and genetic evidence of heterogeneity. *Am J Med Genet* 1989;**33**:209–19.
2. **Kozlowski K,** Beemer FA, Bens G, Dijkstra PF, Iannaccone G, Emons D, Lopez-Ruiz P, Masel J, van Nieuwenhuizen O, Rodriguez-Barrionuevo C. Spondylo-Metaphyseal Dysplasia (Report of 7 cases and essay of classification). *Prog Clin Biol Res* 1982;**104**:89–101.
3. **McKusick VA.** Medical genetics. A 40-year perspective on the evolution of a medical specialty from a basic science. *JAMA* 1993;**270**:2351–6.
4. **Hoo JJ,** Oliphant M. Two sibs with brachyolmia type Hobaek: five year follow-up through puberty. *Am J Med Genet A* 2003;**116A**:80–4.
5. **Rock MJ,** Prenen J, Funari VA, Funari TL, Merriman B, Nelson SF, Lachman RS, Wilcox WR, Reyno S, Quadrelli R, Vaglio A, Owsianik G, Janssens A, Voets T, Ikegawa S, Nagai T, Rimoin DL, Nilius B, Cohn DH. Gain-of-function mutations in TRPV4 cause autosomal dominant brachyolmia. *Nat Genet* 2008;**40**:999–1003.
6. **Dai J,** Cho TJ, Unger S, Lausch E, Nishimura G, Kim OH, Superti-Furga A, Ikegawa S. TRPV4-pathy, a novel channelopathy affecting diverse systems. *J Hum Genet* 2010;**55**:400–2.
7. **Doi H,** Yoshida K, Yasuda T, Fukuda M, Fukuda Y, Morita H, Ikeda S, Kato R, Tsurusaki Y, Miyake N, Saitsu H, Sakai H, Miyatake S, Shiina M, Nukina N, Koyano S, Tsuji S, Kuroiwa Y, Matsumoto N. Exome sequencing reveals a homozygous SYT14 mutation in adult-onset, autosomal-recessive spinocerebellar ataxia with psychomotor retardation. *Am J Hum Genet* 2011;**89**:320–7.
8. **Tsurusaki Y,** Okamoto N, Ohashi H, Kosho T, Imai Y, Hibi-Ko Y, Kaname T, Naritomi K, Kawame H, Wakui K, Fukushima Y, Homma T, Kato M, Hiraki Y, Yamagata T, Yano S, Mizuno S, Sakazume S, Ishii T, Nagai T, Shiina M, Ogata K, Ohta T, Niikawa N, Miyatake S, Okada I, Mizuguchi T, Doi H, Saitsu H, Miyake N, Matsumoto N. Mutations affecting components of the SWI/SNF complex cause Coffin-Siris syndrome. *Nat Genet* 2012;**44**:376–8.
9. **Noordam C,** Dhir V, McNelis JC, Schlereth F, Hanley NA, Krone N, Smeitink JA, Smeets R, Sweep FC, Claahsen-van der Grinten HL, Arlt W. Inactivating PAPSS2 mutations in a patient with premature pubarche. *N Engl J Med* 2009;**360**:2310–18.

10. **Ohnishi Y,** Tanaka T, Ozaki K, Yamada R, Suzuki H, Nakamura Y. A high-throughput SNP typing system for genome-wide association studies. *J Hum Genet* 2001;**46**:471–7.
11. **Holbrook JA,** Neu-Yilik G, Hentze MW, Kulozik AE. Nonsense-mediated decay approaches the clinic. *Nat. Genet* 2004;**36**:801–8.
12. **Ahmad M,** Haque MF, Ahmad W, Abbas H, Haque S, Krakow D, Rimoin DL, Lachman RS, Cohn DH. Distinct, autosomal recessive form of spondyloepimetaphyseal dysplasia segregating in an inbred Pakistani kindred. *Am J Med Genet* 1998;**78**:468–73.
13. **Faiyaz ul Haque M,** King LM, Krakow D, Cantor RM, Rusiniak ME, Swank RT, Superti-Furga A, Haque S, Abbas H, Ahmad W, Ahmad M, Cohn DH. Mutations in orthologous genes in human spondyloepimetaphyseal dysplasia and the brachymorphic mouse. *Nat Genet* 1998;**20**:157–62.
14. **Leroy JG,** Leroy BP, Emmery LV, Messiaen L, Spranger JW. A new type of autosomal recessive spondyloepiphyseal dysplasia tarda. *Am J Med Genet A* 2004;**125A**:49–56.
15. **Krakow D,** Vriens J, Camacho N, Luong P, Deixler H, Funari TL, Bacino CA, Irons MB, Holm IA, Sadler L, Okenfuss EB, Janssens A, Voets T, Rimoin DL, Lachman RS, Nilius B, Cohn DH. Mutations in the gene encoding the calcium-permeable ion channel TRPV4 produce spondylometaphyseal dysplasia, Kozlowski type and metatropic dysplasia. *Am J Hum Genet* 2009;**84**:307–15.
16. **Nishimura G,** Dai J, Lausch E, Unger S, Megarbané A, Kitoh H, Kim OH, Cho TJ, Bedeschi F, Benedicenti F, Mendoza-Londono R, Silengo M, Schmidt-Rimpler M, Spranger J, Zabel B, Ikegawa S, Superti-Furga A. Spondylo-epiphyseal dysplasia, Maroteaux type (pseudo-Morquio syndrome type 2), and parastremmatic dysplasia are caused by TRPV4 mutations. *Am J Med Genet A* 2010;**152A**:1443–9.
17. **Unger S,** Lausch E, Stanzial F, Gillessen-Kaesbach G, Stefanova I, Di Stefano CM, Bertini E, Dionisi-Vici C, Nilius B, Zabel B, Superti-Furga A. Fetal akinesia in metatropic dysplasia: The combined phenotype of chondrodysplasia and neuropathy? *Am J Med Genet A* 2011;**155A**:2860–4.

PAPSS2 mutations cause autosomal recessive brachyolmia

Noriko Miyake, Nursel H Elcioglu, Aritoshi Iida, et al.

J Med Genet 2012 49: 533-538 originally published online July 11, 2012
doi: 10.1136/jmedgenet-2012-101039

REPORT

Exome Sequencing Reveals a Homozygous *SYT14* Mutation in Adult-Onset, Autosomal-Recessive Spinocerebellar Ataxia with Psychomotor Retardation

Hiroshi Doi,[1,2] Kunihiro Yoshida,[3] Takao Yasuda,[4] Mitsunori Fukuda,[4] Yoko Fukuda,[5] Hiroshi Morita,[6] Shu-ichi Ikeda,[6] Rumiko Kato,[7] Yoshinori Tsurusaki,[1] Noriko Miyake,[1] Hirotomo Saitsu,[1] Haruya Sakai,[1] Satoko Miyatake,[1] Masaaki Shiina,[8] Nobuyuki Nukina,[9] Shigeru Koyano,[2] Shoji Tsuji,[5] Yoshiyuki Kuroiwa,[2] and Naomichi Matsumoto[1,*]

Autosomal-recessive cerebellar ataxias (ARCAs) are clinically and genetically heterogeneous disorders associated with diverse neurological and nonneurological features that occur before the age of 20. Currently, mutations in more than 20 genes have been identified, but approximately half of the ARCA patients remain genetically unresolved. In this report, we describe a Japanese family in which two siblings have slow progression of a type of ARCA with psychomotor retardation. Using whole-exome sequencing combined with homozygosity mapping, we identified a homozygous missense mutation in *SYT14*, encoding synaptotagmin XIV (SYT14). Expression analysis of the mRNA of *SYT14* by a TaqMan assay confirmed that *SYT14* mRNA was highly expressed in human fetal and adult brain tissue as well as in the mouse brain (especially in the cerebellum). In an in vitro overexpression system, the mutant SYT14 showed intracellular localization different from that of the wild-type. An immunohistochemical analysis clearly showed that SYT14 is specifically localized to Purkinje cells of the cerebellum in humans and mice. Synaptotagmins are associated with exocytosis of secretory vesicles (including synaptic vesicles), indicating that the alteration of the membrane-trafficking machinery by the *SYT14* mutation may represent a distinct pathomechanism associated with human neurodegenerative disorders.

Hereditary ataxias are genetically heterogeneous neurological disorders: autosomal-dominant, autosomal-recessive, X-linked, and mitochondrial types are known. Among ataxias, spinocerebellar ataxia (SCA) is relatively common and involves the cerebellum, brainstem, or spinocerebellar long tracts.[1] Autosomal-recessive cerebellar ataxias (ARCAs) are generally associated with diverse neurological and nonneurological attributes, resulting in complex phenotypes. ARCAs include congenital nonprogressive ataxias and progressive ataxias such as SCAs.[2] The clinical onset of ARCAs usually occurs before the age of 20, even if congenital types are excluded.[1,3,4] Currently, more than 20 defective genes have been identified in ARCAs.[2,5,6] These genes have variable recognized functions, including those involving mitochondrial energy generation, cellular metabolisms, DNA repair, chaperone-mediated protein folding, RNA processing, and ion channels.[1,3,6] Approximately half of the patients with ARCAs remain genetically unresolved.[4] Therefore, more investigations of ARCAs are required. In this study, we describe a Japanese family with two siblings showing psychomotor retardation and the slowly progressive type of SCA without involvement of pyramidal tracts or peripheral nerves. Exome sequencing combined with homozygosity mapping successfully identified a causative mutation.

Clinical information and blood materials were obtained from the family members after written informed consent was secured. Experimental protocols were approved by IRBs of the Yokohama City University and the Shinshu University. Among the children of first-cousin parents, two siblings (IV-3 and IV-4) were found to be affected, whereas the other two (IV-1 and IV-2) were healthy (Figure 1A). No similar patients were recognized within the family. IV-3 had mild psychomotor retardation from childhood. He found a job after graduating from an ordinary junior high school. At 35 years of age, he lost his job for social reasons. Although he had some gait disturbances from childhood, he could independently go shopping and walk a dog even after leaving his occupation. At the age of ~56, he developed obvious gait unsteadiness and began to stumble frequently. At 58, he started to choke on food. These symptoms gradually worsened, and he sought medical examination at 59 years of age. He displayed disturbances of smooth-pursuit eye movements, dysarthria, mild limb ataxia, and moderate truncal ataxia. His muscle tone was normal, and no involuntary

[1]Department of Human Genetics, Graduate School of Medicine, Yokohama City University, 3-9 Fukuura, Kanazawa-ku, Yokohama 236-0004, Japan; [2]Department of Clinical Neurology and Stroke Medicine, Graduate School of Medicine, Yokohama City University, 3-9 Fukuura, Kanazawa-ku, Yokohama 236-0004, Japan; [3]Division of Neurogenetics, Department of Brain Disease Reseach, Shinshu University School of Medicine, 3-1-1 Asahi, Matsumoto, Nagano 390-8621, Japan; [4]Laboratory of Membrane Trafficking Mechanisms, Department of Developmental Biology and Neuroscience, Graduate School of Life Sciences, Tohoku University, Aobayama, Aoba-ku, Sendai, Miyagi 980-8578, Japan; [5]Department of Neurology, Graduate School of Medicine, The University of Tokyo, 7-3-1 Hongo, Bunkyo-ku, Tokyo 113-8655, Japan; [6]Department of Medicine (Neurology & Rheumatology), Shinshu University School of Medicine, 3-1-1 Asahi, Matsumoto, Nagano 390-8621, Japan; [7]Department of Pediatrics, National Higashi-Saitama Hospital, 4147 Kurohama, Hasuda 349-0196, Japan; [8]Department of Biochemistry, Graduate School of Medicine, Yokohama City University, 3-9 Fukuura, Kanazawa-ku, Yokohama 236-0004, Japan; [9]Laboratory for Structural Neuropathology, Brain Science Institute, RIKEN, 2-1 Hirosawa, Wako 351-0198, Japan
*Correspondence: naomat@yokohama-cu.ac.jp
DOI 10.1016/j.ajhg.2011.07.012.

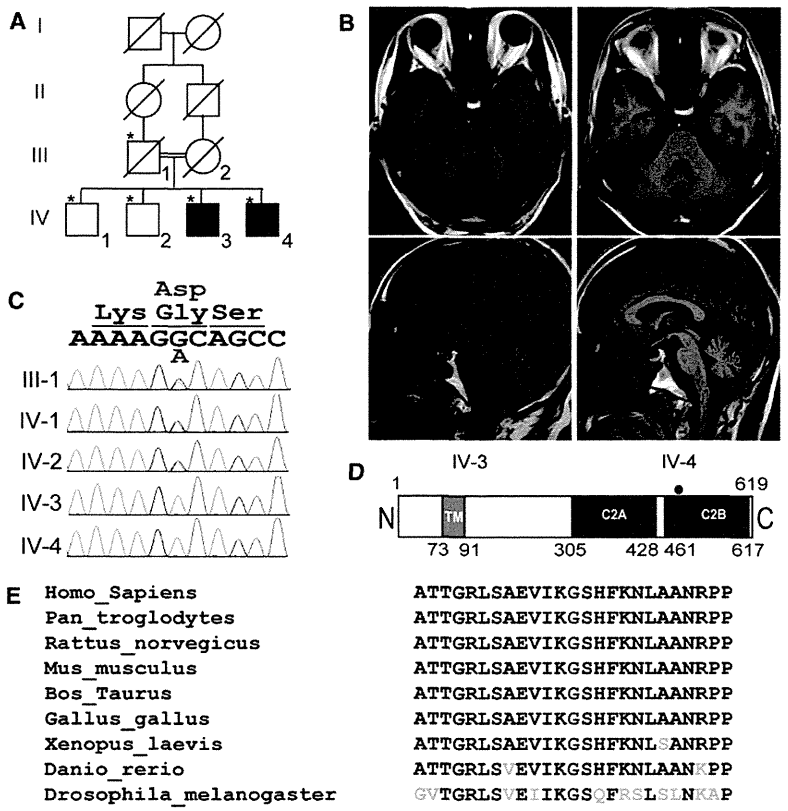

Figure 1. Familial Pedigree, Brain MRI of Patients, and the *SYT14* Mutation Identified

(A) Familial pedigree of the patients with autosomal-recessive spinocerebellar ataxia. *An asterisk indicates members whose genomic DNA was available for this study.

(B) Brain MRI of IV-3 at 59 years of age (left panels) and IV-4 at 56 years of age (right panels). Axial (upper panels) and sagittal (lower panels) sections of a T1-weighted image are shown.

(C) Electropherograms of unaffected (III-1, IV-1, and IV-2) and affected (IV-3 and IV-4) members, who show the mutation.

(D) Schematic presentation of SYT14. The red dot indicates the location of the mutation in the C2B domain.

(E) The missense mutation occurred at an evolutionarily conserved amino acid (in red).

movements were observed. Laboratory examination, including analysis of serum albumin, vitamin E, and α-fetoprotein, was normal. A nerve-conduction study (NCS) indicated no neuropathy. No retinitis pigmentosa was recognized by ophthalmologic evaluation. Brain magnetic resonance imaging (MRI) revealed mild atrophy of the cerebellar vermis and hemispheres but no apparent atrophy of the brain stem or the cerebral cortex. (Figure 1B, left panels).

Similar to IV-3, IV-4 also had psychomotor retardation from childhood, but this retardation was more severe than that of IV-3. After graduation from a school for disabled children at the age of 15, he entered a facility for disabled people. He showed gait disorder, but he was able to walk without a cane. At an age of ~50, his gait disturbance worsened, and he went for a medical check at a hospital when he was 56 years old. He displayed disturbance of smooth-pursuit eye movements, gaze-evoked horizontal nystagmus, dysarthria, mild limb ataxia, and moderate truncal ataxia. No involuntary movements were observed. His laboratory tests, including those for serum albumin, vitamin E, and α-fetoprotein, were normal. NCS was normal. A brain MRI was similar to that of IV-3 (Figure 1B, right panels). The clinical manifestations of these two patients are summarized in Table 1.

To search for the disease locus, we conducted genome-wide SNP genotyping of III-1, IV-1, IV-2, IV-3, and IV-4 by using the Genome-wide Human SNP Array 6.0 (SNP 6.0 array) (Affymetrix, Inc., Santa Clara, CA) according to the manufacturer's instructions. Then, SNP 6.0 array data were subjected to homozygosity mapping with HomozygosityMapper software.[7] For the linkage analysis, a subset of 7339 SNPs with high heterozygosity (mean heterozygosity 0.49) was extracted from the SNP 6.0 array data with the program Linkdatagen, for which the bin size was set to 0.5cM and the allele frequency of the Japanese population was used.[8] The multipoint LOD score was calculated with Allegro version 2[9] on the basis of the model of autosomal-recessive and X-linked-recessive inheritance, respectively. In both models, complete penetrance and a disease-allele frequency of 0.0001 were adopted. The homozygosity mapping revealed a total of three regions, which together were approximately 11.35 Mb in size, as candidate loci, where genes known to be mutated in ARCA did not exist (Table 2). In the model of autosomal-recessive inheritance, a total of ten regions with a LOD score greater than 1.5 in the multipoint linkage analysis were identified (Table S1). The three homozygous regions in accordance with the linked regions still survived as candidate regions. On the basis of X-linked recessive inheritance, a total of three regions with positive LOD scores (maximum LOD score = 0.9031) were highlighted; together, these three regions were approximately 101.03 Mb (Table S1).

To find a gene mutation within the candidate loci, we performed whole-exome sequencing on IV-3 and IV-4. Three micrograms of genomic DNA was processed with the SureSelect Human All Exon Kit v.1 (approximately 180,000 exons covering 38 Mb of the CCDS database) (Agilent Technologies, Santa Clara, CA) according to the manufacturer's instructions. Captured DNAs were sequenced on an Illumina GAIIx (Illumina, San Diego, CA) with 76 bp pair-end reads. Of the possible eight lanes of the flow cell, two lanes for IV-3 and three lanes for IV-4 (Illumina) were used. Image analysis and base calling

Table 1. Clinical Features of the Patients

Clinical Features	IV-3	IV-4
Age at present	61	58
Sex	male	male
Age of obvious ataxia	56	around 50
Mental retardation	mild	moderate
Ocular apraxia	no	no
Ophthalmoplegia	no	no
Nystagmus	no	+
Dysarthria	+	+
Truncal ataxia	++	++
Limb ataxia	+	+
Extrapyramidal signs	no	no
Involuntary movements	no	no
Sensory involvements	no	no
Tendon reflex	normal-increased	normal-decreased
Plantar responses	normal	normal
Peripheral neuropathy	no	no
Pes cavus	no	no
SARA[a]	12/40	15/40
Cerebellar atrophy on MRI	+	+
others	normal level of serum albumin, vitamin E, and α-fetoprotein	normal level of serum albumin, vitamin E, and α-fetoprotein

[a] SARA: Scale for the assessment and rating of ataxia.[32]

Table 2. Regions of Homozygosity

Chromosome	Chromosomal Position (rsID)	Size (Mb)	LOD
1	207226930 (rs2761781)–213992561 (rs1857229)	6.77	2.0537
4	181929079 (rs918401)–185188999 (rs7690914)	3.26	2.0554
22	45676443 (rs3905396)–47003473 (rs2013591)	1.33	2.0545

Regions of homozygosity were identified by HomozygosityMapper, and the LOD scores were calculated by multipoint linkage analysis, for which SNPs were extracted from SNP 6.0 array data via Linkdatagen.

were performed by sequence control software (SCS) real-time analysis (Illumina) and CASAVA software v1.6 (Illumina). Reads were aligned to the human reference genome sequence (UCSC hg18, NCBI build 36.1) via the ELAND v2 program (Illumina). Coverage was calculated statistically with a script created by BITS (Tokyo, Japan). Approximately 71 million reads from IV-3 and 148 million reads from IV-4 (these numbers of reads passed quality-control [Path Filter]) were mapped to the human reference genome with Mapping and Assembly with Qualities (MAQ)[10] and NextGENe software v2.00 (SoftGenetics, State College, PA) under the default settings. MAQ aligned 59,491,138 and 126,159,746 reads to the whole genome for IV-3 and IV-4, respectively. A script created by BITS was used for extraction of SNPs and indels from the alignment data; dbSNP build 130 served as a reference for registered SNPs. A consensus quality score of 40 or more was adopted for the SNP analysis in MAQ. Coverage analysis revealed that 65.0% (IV-3) and 71.3% (IV-4) of the coding sequences (CDS) were completely covered (100%), and 77.7% (IV-3) and 80.3% (IV-4) of CDS were mostly covered by reads (90% or more) through the whole genome. 79.0% (IV-3) and 79.7% (IV-4) of total CDS were covered by ten reads or more (50 reads or more in 66.4% and 77.1%, respectively).

To identify the pathogenic mutation, we adopted a prioritization scheme, which has been used in recent studies.[11–13] First, we excluded the variants registered in dbSNP130 from all the detected variants and then picked up homozygous mutations and variants in coding regions and the intronic regions within 50 bp from coding sequences. Of the homozygous mutations and variants, we focused on those within the candidate regions. As a result, only two missense mutations or variants, p.Gly484Asp (c.1451G>A) (NM_001146261.1) in exon 8 of *SYT14* (1q32.2, [MIM 610949]) and p.Gln4203Arg (c.12608A>G) (NM_206933.2) in exon 63 of *USH2A* (1q41, [MIM 608400]) remained as candidates for both cases (Table S2). Sanger sequencing with ABI 3500xL (Life Technologies, Carlsbad, CA) confirmed that the c.1451G>A of *SYT14* was homozygous in IV-3 and IV-4 and heterozygous in III-1 (father), IV-1, and IV-2, whereas the c.12608A>G of *USH2A* was homozygous in IV-2 as well as IV-3 and IV-4 (Figure 1C and data not shown). The *SYT14* missense mutation occurred at an evolutionarily conserved amino acid among different species and resides in the second C2 (C2B) domain (Figures 1D and 1E). In silico analysis incorporating different tools, including Polyphen, Polyphen2, SIFT, and Align GVGD, consistently indicated that the change was damaging (Table S3). The mutation was not detected in 576 Japanese control chromosomes, indicating that the mutation is very rare. On the basis of the X-linked recessive model, no pathological hemizygous mutation of protein-coding genes was detected in the possible candidate loci (Table S4).

We considered the *SYT14* mutation to be the causative agent and used the Sanger method to conduct mutation screening of all the coding regions of *SYT14* in 65 simplex SCA cases and 37 SCA familial cases, including three with autosomal-recessive inheritance. Only p.Gly183Glu (c.548G>A) was found in one family with autosomal-dominant SCA; however, the change was not consistent with the SCA phenotype in the family (Table S3). Thus, we could not detect any other pathological changes in *SYT14*. This was probably due to the small number of cases tested.

Synaptotagmin XIV (SYT14), which is encoded by *SYT14*, is a member of the synaptotagmins (SYTs), which are membrane-trafficking proteins, and SYT14 is conserved across many organisms.[14] Although the original report indicated that *SYT14* was not expressed in mouse brain,[14] multiple lines of evidence, including from the Allen brain Atlas, suggest that *SYT14* is expressed in the central nervous system (CNS) of the fly, mouse, and human brains.[15,16] To confirm *SYT14* expression in the CNS, we performed TaqMan quantitative real-time PCR analysis with cDNAs of adult human tissue (Human MTC Panel I, #636742) (Clontech Laboratories, Mountain View, CA), fetal human tissue (Human Fetal MTC Panel, #636747) (Clontech Laboratories), mouse tissue (Mouse MTC Panel I, #636745) (Clontech Laboratories), and various regions of the mouse brain (GSMBRSET) (NIPPON Genetics, Tokyo, Japan) as templates. Predesigned TaqMan probe sets for human *SYT14* (Hs00950169_m1), mouse *Syt14* (Mm00805319_m1), human *β-actin* (*ACTB*, 4326315E), and mouse *Actb* (43522341E) from Applied Biosystems were used. PCR reactions (total volume of 20 μl) contained 10 μl of the TaqMan Gene Expression Master Mix (Applied Biosystems), 1 μl of 20 × TaqMan reagents for *ACTB/Actb* and *SYT14/Syt14*, and 1 μl of cDNA (containing 1 ng cDNA in MTC panels and 25 ng cDNA in GSMBRSET) as the template. PCR was performed on a Rotor-Gene Q (QIAGEN, Valencia, CA) as follows: 2 min at 50°C and 10 min at 95°C, then 40 cycles of 95°C for 15 s and 60°C for 1 min. Expression levels were calculated with the Rotor-Gene Q Series Software (QIAGEN) by the $2^{-\Delta\Delta Ct}$ method. The cycling threshold (Ct) of the target gene was compared with the Ct of *ACTB* cDNA, and ΔCt was expressed as Ct of *SYT14* − Ct of *ACTB*. ΔΔCt was expressed as ΔCt of the control sample − ΔCt of each sample, and relative concentration was determined as $2^{-\Delta\Delta Ct}$. Expression in the kidney and the cerebral cortex was used as the control in Figures 2A–2D. *SYT14* was predominantly expressed in human adult and fetal brain tissues (Figures 2A and 2B). Even in mice, substantial expression in the brain was confirmed (but, not predominant) (Figure 2C). Among various brain regions in mice, *SYT14* was mostly expressed in the cerebellum (Figure 2D).

Intracellular distribution of SYT14 in cultured cells was investigated. The full-length *SYT14* PCR product amplified from human brain cDNA (MHS4426-99239810, Open Biosystems, Huntsville, AL) was used as a template and subcloned into pDONR221 (the entry vector of Gateway system, Invitrogen). We used site-directed mutagenesis to produce the *SYT14* mutant and variants by using a mutagenesis kit (Toyobo, Osaka, Japan). Variants include c.611C>T and c.810_812del, which are registered in dbSNP130, and c.548G>A, which was detected in an SCA patient with autosomal-dominant inheritance but did not segregate with the phenotype, indicating that it is nonpathogenic (Table S3). All constructs were verified by DNA sequencing. Each construct was recloned into the pEF-DEST51 mammalian expression vector (Invitrogen) and transfected to COS-1 cells with the FuGENE^{R}6 transfection reagent (Roche Applied Science, Mannheim, Germany) according to the manufacturer's instructions. Localization of the mutant (p.Gly484Asp) was clearly different from that of the wild-type and other (normal) variants. Whereas the wild-type and other variants were localized to the perinuclear and submembranous regions, p.Gly484Asp was localized in the cytoplasm (significant amounts were in the perinuclear region) but formed a characteristic reticular pattern without showing any submembranous distribution (Figures 2E and S2B). Confocal microscopic analysis showed that the p.Gly484Asp mutant was colocalized with an endoplasmic reticulum (ER) marker, protein disulfide isomerase (PDI), throughout the cells, whereas the wild-type colocalized with PDI dominantly in perinuclear regions (Figure 2F). immunoblot analysis combined with subcellular fractionation of the transfected cells further confirmed that the mutant was distributed differently from the wild-type. The wild-type and the mutant (p.Gly484Asp) were distributed in the nucleus and Golgi apparatus fractions; however, only the mutant was detected in microsome fractions containing ER fragments together with an ER membrane marker, calnexin (Figure S1).[17] These data suggest that improper folding of the mutant protein results in abnormal retention in the ER.

To investigate the effect of the p.Gly484Asp mutation in the C2B domain on phospholipid binding activity, we amplified cDNA of C2B domains from the wild-type and the p.Gly484Asp mutant from SYT14-expressing vectors by using the following primers: sense, 5′-GGATCCGAAA GTACATCCTCATGTCA-3′; and antisense, 5′-TCATGAC TCTAGCAACGCAT-3′. We then recloned the cDNA into *Escherichia coli* (*E. coli*) expressing vector (pGEX-4T-3). The C2B domain of SYT14 fused to glutathione S-transferase (GST) was expressed in *E. coli* JM109 and purified by standard protocols. Both GST-SYT14-C2B (WT) and GST-SYT14-C2B (p.Gly484Asp) could be mostly purified of contamination by degradation products, but the amount of GST-SYT14-C2B (p.Gly484Asp) obtained was at least four times smaller than that of GST-SYT14-C2B (WT) (data not shown). Liposome (phosphatidylcholine and phosphatidylserine, 1:1, w/w) cosedimentation assay with purified GST-SYT14-C2B was performed as described previously.[18] The result showed that the SYT14-C2B (p.Gly484Asp) bound liposomes similarly to SYT14-C2B (WT) (Figure 2G), indicating that the p.Gly484Asp mutation had no effect on the Ca^{2+}-independent phospholipid-binding activity of the SYT14-C2B domain.

The Allen Mouse Brain Atlas indicates that *Syt14* is expressed in Purkinje cells of the cerebellum in mice; however, SYT14 localization has not been fully investigated.[15] A rabbit polyclonal anti-SYT14 antibody (Ab-SYT14) was generated for immunoblotting and immunocytochemistry (Operon Biotechnologies, Tokyo, Japan) (Figure S2). Immunohistochemical analysis of mouse and human brains was

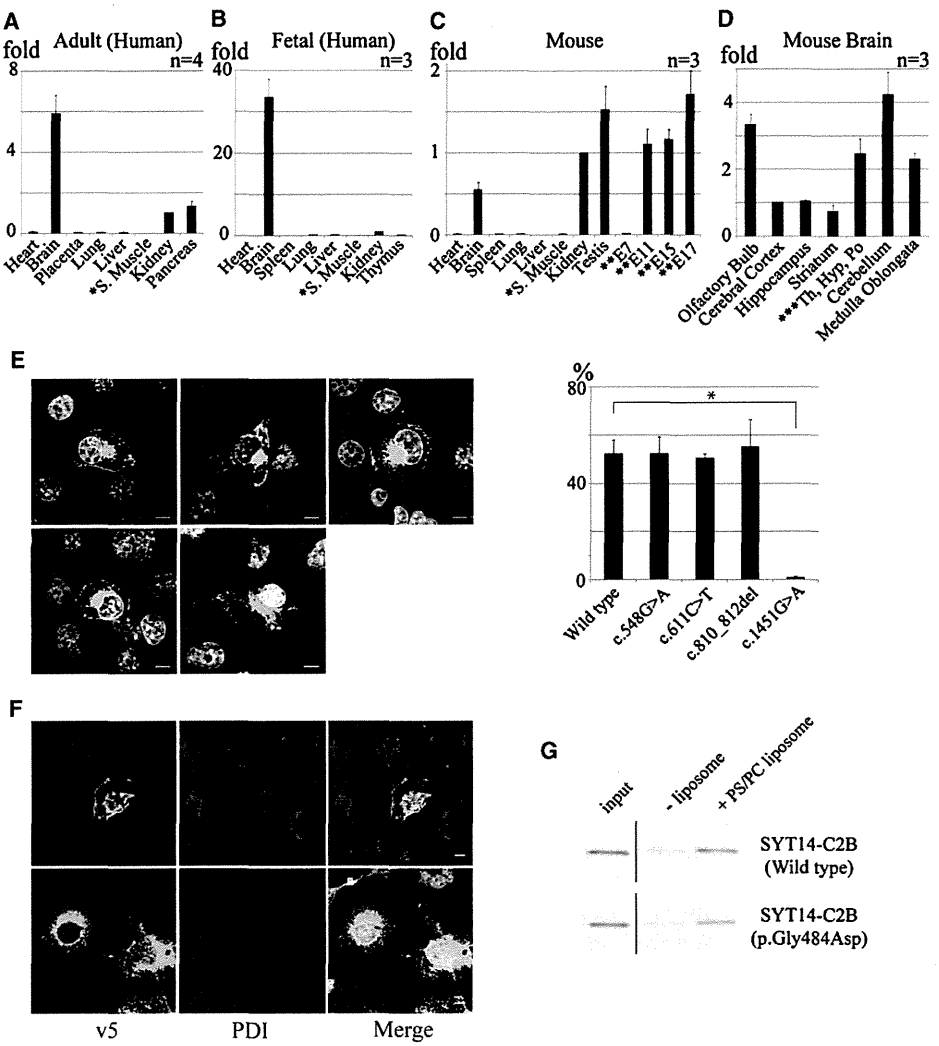

Figure 2. Expression Studies of *SYT14/Syt14* cDNA in Human and Mouse Tissues and Localization of SYT14 in Transfected COS-1 Cells
(A–D) The results of a TaqMan quantitative real-time PCR assay in which the first-strand cDNA of human adult tissues (A), human fetal tissues (B), mouse tissues (C), and various regions of mouse brain (D) were used as templates. The relative cDNA concentrations were determined from cDNA concentrations of the kidney (human adult tissues, human fetal tissues, and mouse tissues) or cerebral cortex (various regions of the mouse brain). Error bars represent the standard deviation. *S. Muscle indicates skeletal muscle. **E7, **E11, **E15, and **E17 indicate mouse embryos at 7, 11, 15, and 17 days of embryonic development, respectively. ***Th, Hyp and Po indicate thalamus, hypothalamus, and pons.
(E) Immunocytochemistry of COS-1 cells transfected with expression vectors of v5/His-tagged wild-type (upper left), p.Gly183Glu (c.548G>A) (upper middle), p.Pro203Leu (c.611C>T) (upper right), p.Glu270del (c.810_812del) (lower left), or p.Gly484Asp (c.1451G>A) (lower middle) SYT14. The SYT14 was detected with the anti-v5 antibody (Alexa fluor 488 as the secondary antibody). Nuclei were stained (white) with 4′,6-diamidino-2-phenylindole (DAPI). The horizontal bars indicate 10 μm. The bar graph indicates the ratio of the cells in which overexpressed proteins were accumulated in submembranous regions. A total of 120 cells per each transfectant in triplicated experiments were counted. Submembranous localization of the mutant (p.Gly484Asp) was mostly unseen, in contrast to the wild-type (*$p < 0.001$).
(F) Immunocytochemical analysis of COS-1 cells transfected with expression vectors of v5/His-tagged wild-type (upper panels) or the p.Gly484Asp mutant (lower panels). The SYT14 was detected with the anti-v5 antibody (Alexa fluor 488 as the secondary antibody), and PDI (protein disulfide isomerase) was visualized with an anti-PDI antibody (Alexa fluor 546 as the secondary antibody). Nuclei were stained (white) with DAPI. The scale bar represents 10 μm. The anti-v5 and anti-PDI antibodies and the Alexa-488-conjugated secondary antibody were all used at a dilution of 1:1000.
(G) Phospholipid binding activity of the C2B domain of the wild-type SYT14 and the p.Gly484Asp mutant. Liposomes and GST-fusion proteins (2 μg) were incubated in 50 mM HEPES-KOH (pH 7.2) in the presence of 2 mM EGTA for 15 min at room temperature. After centrifugation at 12,000 × *g* for 10 min, the supernatants (non-binding fraction) and pellets (phospholipid-binding fraction) were separated as described previously.[18] The pelleted samples and input samples (100 ng) were subjected to 10% SDS-PAGE followed by immunoblotting with horseradish peroxidase-conjugated anti-GST antibody (Santa Cruz Biotechnology, Santa Cruz, CA).